13th International Symposium on Particle Image Velocimetry – ISPIV 2019
Munich, Germany, July 22-24, 2019

Effects of Periodic Inflow Turbulence on the Statistics in the Wake of a Linear LPT Cascade at Jet-Engine relevant Test Conditions

Martin Bitter[1*], **Reinhard Niehuis**[1]

[1] Bundeswehr University Munich, Institute of Jet Propulsion, 85579 Neubiberg, Germany

[*] martin.bitter@unibw.de

Abstract

In this paper, the results from PIV measurements on a linear low-pressure turbine cascade are presented. Two individual test campaigns, which were a) stereoscopic PIV measurements at the inlet and b) phase-locked 2D2C PIV measurements downstream of the cascade, were carried out to characterize the magnitude as well as the temporal development of the effects originating from periodic inflow turbulence on the wake topology downstream of the cascade. The experiments were performed in the High-speed Cascade Wind tunnel located at the Bundeswehr University in Munich. The facility offers the uniqueness to study blade characteristics at jet-engine relevant envelope conditions with respect to Mach- and Reynolds numbers. A wake generator was used to produce unsteady periodic inlet conditions in order to simulate rotor/stator interactions in a turbine stage. The experiments were carried out for two Reynolds numbers Re = $[60; 120]\cdot 10^3$ based on the blade's axial chord length and exit conditions. The results show a periodic increase in the passage's peak turbulence intensity by more than 2 % and an effect on the energy dissipation rate originating from the simulated rotor wakes.

1 Introduction and Motivation

The inflow turbulence is an essential parameter for the design process of airfoils. Depending on the design philosophy, realistic inflow turbulence can lead to a higher aerodynamic loading or a decreased safety margin with respect to separation. Herbst et al. (2017) and Breuer (2018) examine the effect of large-scale inflow turbulence, such as wind gusts, on low-Re airfoils. In turbomachinery, the inflow into rotor and stator stages downstream of the first blade row is periodically influenced by the wakes of the upstream blade rows. The presence of periodic turbulence can lead to a higher aerodynamic loading or a more aggressive blade design, compare e.g. Talan and Hourmouziadis (2002). The Institute of Jet Propulsion of the Bundeswehr University in Munich has a long research track on the experimental and numerical investigation of the effect of steady and periodic turbulent inflow, on secondary flow or separation bubbles at low-pressure turbine cascades, compare e.g. Acton and Fottner (1998), Ciorciari et al. (2014) or Kirik and Niehuis (2015). The institute operates a wind tunnel which can be equipped with a wake generator for the separation of steady and unsteady effects. Further details are discussed later in Chapter 2.
A driving motivation for the work presented in this paper is the generation of a validation data set. A tool for aero-elastic predictions requires the slope of the velocity gradient field as boundary condition. For tracing back and separating the effects of periodically disturbed inflow on the development of the cascades exit flow topology, the inflow vorticity field into the linear cascade originated by moving wakes is investigated separately from the cascade's wake flow field within this paper.
Nowadays, the PIV measurement technique is frequently applied for estimating the turbulent intensity in flows because the statistical variance of the turbulent quantities is typically available from the data. The authors in Scharnowski et al. (2018) estimate their wind tunnel turbulence intensity by means of 2D2C PIV whereas they point out, that a certain dynamic range in the vector shift should be present in order to derive reliable results. Other valuable work, e.g. presented by Gomes-Fernandes et al. (2012) use the PIV technique for the estimation of the statistical quantities of coherent structures from fractal grids. As widely known in the community, the spatial filtering effect as well as the sensitivity to local gradients in the flow

can reduce the precision of the results significantly. The authors in Dróżdż and Uruba (2014) compare the turbulent quantities measured with PIV to reference data acquired with hot-wire anemometry. They show a very good agreement of the statistical quantities from both techniques. Similar work did the authors in Chemnitz and Niehuis (2019), but for exactly the same wind tunnel facility as presented later in the text for these experiments. They demonstrated robust turbulence intensity results from PIV compared to a hot-wire anemometry field of similar spatial resolution in the wake of a low-pressure turbine cascade. The following section introduces the experimental approaches for the presented work. Prior to the discussion of the final results, the expected measurement uncertainty is briefly discussed.

2 Experimental Setup and Methodology

2.1 Wind tunnel setup

The High-speed Cascade Wind tunnel (HGK) of the Institute of Jet Propulsion located at the Bundeswehr University Munich is an open jet facility, as outlined in Figure 1. Key performance features of the facility are described in detail in Scholz and Hopkes (1959) and Sturm and Fottner (1985). A three-stage axial compressor with variable inlet guide vanes as well as the downstream components of the facility are placed inside a pressure chamber. The wind tunnel can be operated at static pressures from 120 kPa down to approx. 4 kPa by evacuating the surrounding vessel with the use of 2 vacuum pumps. This pressure change enables a large Reynolds number range of $2 \cdot 10^5 \leq \mathrm{Re}/l \leq 3.5 \cdot 10^7 [m^{-1}]$. The axial compressor is driven by a 1.8 MW electric motor, which is placed outside the pressure chamber. The electrical power allows a Mach number range of $0.15 \leq \mathrm{Ma} \leq 1.1$ over the entire pressure range. For highest test section Mach numbers the cross section (height H, width W) must be reduced from a maximum of $500\,mm^H \times 300\,mm^W$ down to $250\,mm^H \times 300\,mm^W$. As the total temperature in the settling chamber can also be adjusted by the main air cooler, the Mach and Reynolds number conditions can be controlled independently over the entire range. The turbulence intensity at the inlet of the cascade is tuned to jet-engine relevant conditions by placing turbulence generating grids with varying turbulence intensity in the HGK nozzle. A grid with a turbulence intensity around 4 % was used for the experiments presented here, as depicted in Fig. 2.
A linear low-pressure turbine (LPT) cascade with seven blades was used for these experiments. The design exit Mach number of the cascade $\mathrm{Ma}_{2,th}$ was close to 0.7. The blade's axial chord length l_{ax} as well as the blade's pitch P were about 50 mm. The tests were conducted at 2 Reynolds numbers $\mathrm{Re}_{2,th} = [60; 120] \times 10^3$. The absolute pressure in the vessel was $p_{Ves} \approx [5; 12]$ kPa in order to realize the isentropic exit conditions at an inlet total temperature of $T_t = 303\,K$ for both Re numbers.

2.1.1 Wake Generator

As the turbulence level in a jet engine stator stage is increased by the wakes of the upstream rotor stage(s), an isolated investigation of this effect on the blade's aerodynamic performance can be found e.g. in Walker

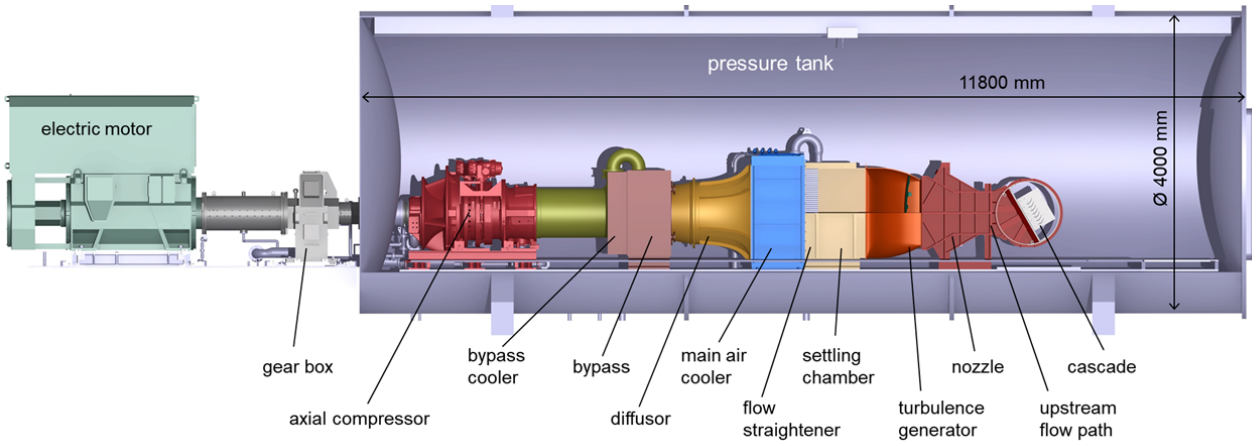

Figure 1: Schematic of the High-speed Cascade Wind tunnel (HGK) at the Bundeswehr University Munich.

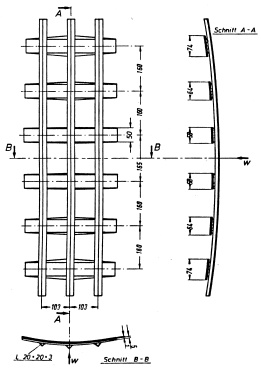

Figure 2: Inflow turbulence grid of the HGK with turbulence intensity $TI \leq 9\,\%$.

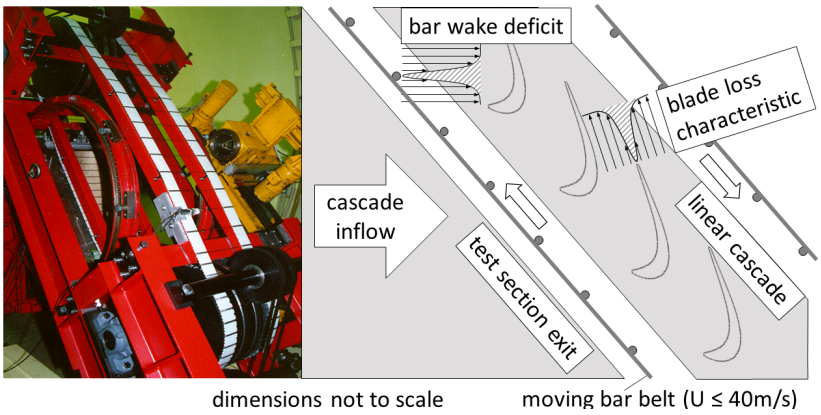

Figure 3: Photograph (*left*) and schematic (*right*) of the wake generator (*EIZ*) placed at the outlet of the HGK test section. The max. circumferential speed of the moving bars is 40 m/s. The dimensions are not to scale.

(1993). For the separation of the effects, a "wake generator" is typically used in cascade testing, compare also Acton and Fottner (1998), Stieger and Hodson (2005) or Mahallati and Sjolander (2012). The test section exit of the HGK can be equipped with such a wake generator, denoted as *EIZ* in the following and presented in Fig. 3. Wakes of upstream rotor stages are simulated by cylindrical steel bars of 2 mm diameter, compare Acton and Fottner (1996). These bars are fixed on two moving belts at changeable bar pitches. The belts rotate continuously in a loop with a maximum circumferential speed of $U = 40\,\mathrm{m/s}$ at pitch $P_{bar} = 80\,\mathrm{mm}$. Hence, a periodic inflow perturbation with a frequency $f = 500\,\mathrm{Hz}$ is generated. It must be stated that, even at relevant axial inflow velocity c_{ax}, it is not possible to realize jet-engine relevant Strouhal numbers Sr or flow coefficients Φ as defined by Eq. 1 due to the speed limits of the device.

$$Sr = \frac{f \cdot l_{ax}}{c_{ax}} = \frac{U}{P_{bar}} \cdot \frac{l_{ax}}{c_{ax}} = \frac{l_{ax}}{P_{bar}} \cdot \frac{1}{\Phi} = 0.26 \tag{1}$$

For relevant conditions of the low-pressure turbine blade investigated here, the turning rate should be at least increased by a factor of 3. Although there are limitations in the rotational speed, the transferability of the results generated with the *EIZ* at a different cascade were shown e.g. by the authors in Brunner and Fottner (1999).

2.1.2 Particle Image Velocimetry

In order to separate the effects, the experimental investigations were carried out in two individual campaigns. The flow field around a bar pitch of the wake generator was characterized by using a stereoscopic PIV setup. These experiments are referred to as *Inflow Investigations* in the following. On the other side, the *Wake Investigations* focus on the effect of the periodic inflow on the topology of the exit flow field downstream the cascade.

Stereoscopic Inflow Measurements

A stereoscopic 2D3C PIV setup was realized in the center plane around a bar pitch, where the wind tunnel flow is 2-dimensional. The major goal of the measurements was the precise quantification of the turbulence intensity TI produced by the bars. As presented in Chemnitz and Niehuis (2019), the estimation of the TI quantities by means of this approach is trustworthy for wake flow fields downstream of a linear cascade. For the sake of better optical access and reduced vibrations of the entire setup, the inflow measurements were carried out while the wake generator was not moving. In order to produce comparable conditions downstream of the resting bar as in the case of a moving bar, the axial inflow velocity was increased by the magnitude of the axial and circumferential components of the bar turning rate. Hence, the inflow velocity bars was $c_{ax} \approx 130\,\mathrm{m/s}$, which was 30 % higher compared to c_{ax} at rotating bars.
Earlier investigations revealed, that the presence of the LPT cascade's potential field downstream of the bar is not strongly essential for the development of the correct downstream flow topology behind the bars. Consequently for better optical access, these experiments were carried out without a linear cascade installed.

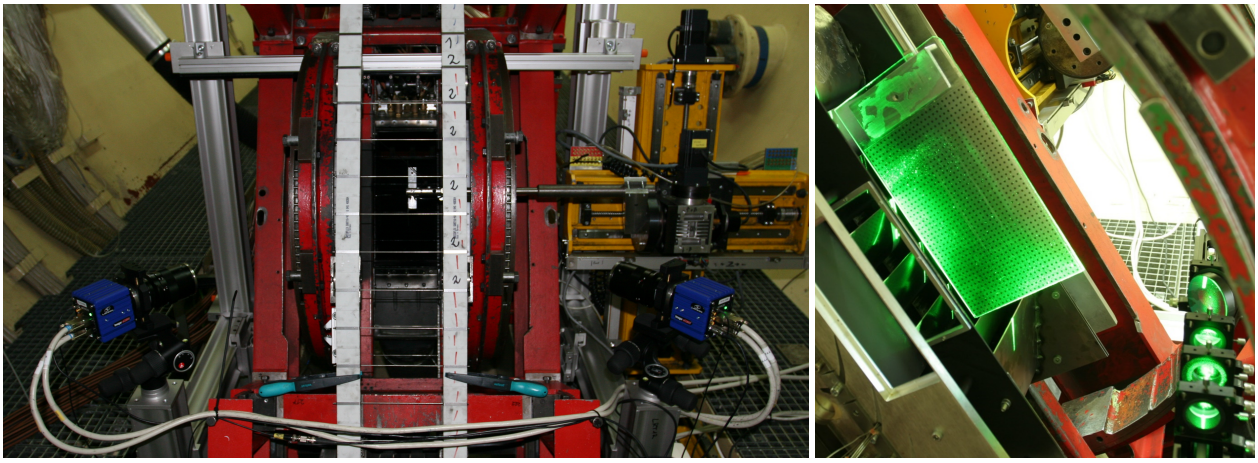

Figure 4: *Left*: Stereoscopic PIV setup downstream of the stationary EIZ; *Right*: Light-sheet optics and camera calibration target for the 2D2C PIV investigations in the center plane downstream of the LPT cascade.

Two 5.5 Mpx sCMOS cameras at Scheimpflug conditions, each equipped with a 50 mm Zeiss Macro Planar lens, were installed at a distance of about 60 cm away from the center plane behind the bars, to be seen on the left in Figure 4. The field of view was calibrated with a transparent calibration target in 5 co-planar planes at $\Delta z = [-2;-1;0;1;2]$ mm around the center plane. A self calibration as included in the state-of-the-art PIV acquisition and processing software DaVis 8.4 in its latest release was performed in order to encounter for remaining disparities. The final remaining disparity in out-of-plane direction was 0.12 mm. The final reconstructed field of view for both cameras was $127\,mm^W \times 105\,mm^H$. Two laskin-type DEHS seeding generators provided a tracer particle density of $PPP = 0.0215 \pm 0.0026$ for the inflow measurements at the lower Reynolds number.
An Innolas Spitlight PIV-1000 Nd:YAG laser with 450 mJ pulse energy per cavity at 532 nm wavelength was applied for light-sheet illumination. A set of 5.000 double-frame images was recorded at 15 Hz for each operating point. The PIV images were pre-processed by subtracting a local Gaussian intensity average as well as by performing a Butterworth low pass filtering with a filter width of 7 images. Unfortunately, the data availability in the vicinity of the bar's surface is reduced due to laser light reflections which could not be removed in the setup or by pre-processing the data. A state-of-the-art multi-pass cross correlation with reducing interrogation window size (IWS, 128^2 px $\rightarrow$ 32^2 px) was used for vector field computation as implemented in Davis 8.4. (For performance validation refer to Kähler et al. (2016).) The spacing of the final vector field was 0.6 mm using a 50 % overlap of the interrogation windows. Finally, a data availability of better than 99.4 % can be assured over a wide range of the vector field for both Reynolds numbers.

Phase-locked Wake Measurements

The focus for the wake measurements was on the separation between the undisturbed flow and the periodic perturbation from the inlet and the corresponding effects on the development of the statistical quantities in the wake flow field downstream of the blades. A standard 2D2C-PIV setup was implemented at mid span behind the 5th and 6th blade of the cascade, as shown on the right of Fig. 4. The field of view of the reconstructed vector field for the 5.5 Mpx sCMOS camera was about $90\,mm^W \times 100\,mm^H$. The image pre-processing and vector field calculation parameter were widely identical to the ones of the inflow measurements, except the final IWS was 48^2 px. Hence, a final vector spacing of 1 mm was reached with 50 % vector overlap.
For a deeper inside in the temporal development of the periodically disturbed flow field, the wake measurements were carried out as phase-locked measurements. One bar passing period $T = 1/500\text{Hz} = 2\,\text{ms}$ was sampled in 10 time steps, each separated by $\tau = 200\,\mu$s. The trigger signal for the phase-locked measurements was generated by an optical counter (Sick KTS-WP9124) which was detecting the negative edges of the passing bars. An ensemble of 1000 PIV double-frame images was processed and averaged for each time step τ. A period-averaged flow field over all time steps was subtracted from the ensemble average of each time step for pointing out the temporal evaluation of the wake flow field in the presence of the periodic inflow perturbations. The representative flow quantities (e.g. turbulence intensity, vorticity or kinematic

energy dissipation rate) were calculated in the main flow's frame of reference, having u and v as the components in stream-wise and normal direction, respectively. The transformation was performed by rotating the flow field around the integral vector angle of the period averaged flow field. As the Mach number behind the LPT cascade increases compared to the inlet, a lower tracer density is also expected. The concentration was $PPP = 0.0085 \pm 0.0018$ for the lower Reynolds number.

2.1.3 Measurement Uncertainty

Turbulent quantities from PIV

As the ambient pressure in the chamber around the wind tunnel is significantly reduced, the PIV particle's following behavior around a turbine blade was assessed numerically in Bitter et al. (2016). It was shown, that the density change had negligible influence on the particle response so that the PIV technique can deliver reliable results at low-Re conditions in the HGK. The number of PIV samples in these experiments seems sufficient for a converged estimation of the statistical quantities, which are the basis for the calculation of the turbulence intensity in both, the inflow and the wake measurements, as indicated by the convergence in Fig. 5. The residual change of all 3 fluctuation components for the inflow field is less than 10^{-2} %, and similar is the statistical error for more than 1.000 samples. A variation of the IWS quantifies the influence of the spatial filtering effect. As the interrogation windows become too small, the noise increases as a consequence of reduced statistical robustness due to low PPP and increased local gradients. If the IWS are too large, the dominant structures are damped out. In the case of the inflow measurements, it is expected that the dominant structures originate either from the turbulence grid or from the bars. Assuming a vortex-shedding dominated Sr number of 0.21 and the respective characteristic length scales for both dominating obstacles in the flow, frequencies of 200 Hz are expected for the grid structures and around 14 kHz for a bar, respectively. Converting these frequencies into length scales by applying Taylors frozen pattern hypothesis using the local convection velocity, the structure size will range from approx 9 mm up to some ten centimeters. A comparison of the TI values extracted from the PIV results at a point in the free-stream of the flow field to the reference value from a hotwire measurement taken from a previous test campaign at a point in the inlet of the same LPT cascade shows a good agreement in TI over a wide range of interrogation windows. The results of the tripple hot-wire probe with spatial dimensions of 1.9 mm would exactly match an IWS of 96 px with the same spatial resolution. An IWS of 32 or 48 px still serves a good compromise between a required spatial resolution and the spatial filtering effect.

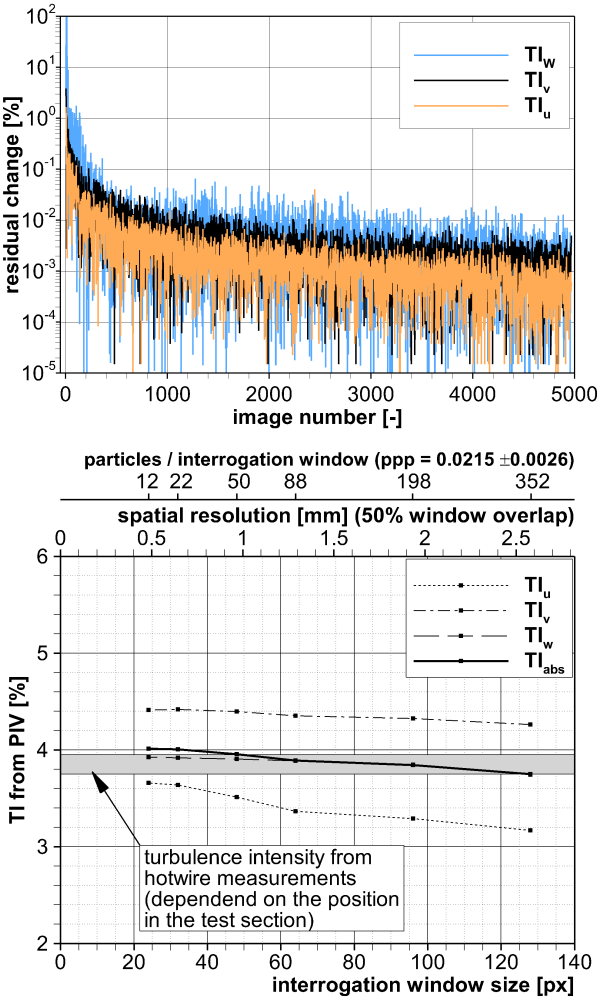

Figure 5: Residual change of the three turbulence intensity components TI_u, TI_v & TI_w extracted from the free-stream velocity fluctuations measured with 2D3C PIV.

Precision of wind tunnel operating point

Turbine blades or cascades are typically designed for an aerodynamic reference condition (ADP, fixed $Ma_{2,th}$ and $Re_{2,th}$) at the exit of the blade. For the HGK wind tunnel facility, this requires the precise and stable setting of the total inlet pressure pt_1, the ambient pressure in the chamber p_{Ves} and the total temperature T_t. The only absolute pressure

Measurement Value	Sensor	full-scale (FS)	FS error	Precision
plenum pressure $p_\infty - p_{Ves}$	Mensor/WIKA CPT 6 series	100 kPa	$\pm$7.5 Pa	$\leq$ 0.2 kPa
dynamic pressure $pt_1 - p_{Ves}$	Mensor/WIKA CPT 6 series	75 kPa	$\pm$10 Pa	$\leq$ 0.1 kPa
total temperature T_{t1}	TC Pt100 RTD (calibrated)	0 – 100 °C	$\pm$0.2 K	$\leq$ 0.4 K
RPM axial compressor	Braun Tacho A5 rev. sensor	$\leq$ 25 kHz	$\pm$0.01 %	$\leq$ 0.05 %

Table 1: Summary of the installed sensors and their precision limits for controlling the High-speed Cascade Wind tunnel operating conditions.

measurement is performed for the ambient pressure in the lab p_∞. All remaining pressures are measured as differential pressure. Table 1 informs about the sensor type, which is used for the control of the operating point, as well as their full scale FS, the FS error and the precision of adjustment. The total temperature T_{t1} is measured in the settling chamber by means and averaged from four calibrated PT100 resistance thermometers. The adjustment of the cooling water flow in combination with the homogeneity of the main air cooler leads to a temperature precision of adjustment of $\leq$ 0.4 K. The revolutions of the axial compressor are monitored indirectly by measuring the DC motor revs by means of a Braun Tacho A5 sensor. The final stability is better than 0.05 % at 12.500 rpm (110 % compressor speed).

3 Results of the Inflow Investigations

The ensemble-averaged results from the inflow measurements at Re = 60.000 and Re = 120.000 are shown in Figure 6 for the absolute velocity and the turbulence intensity. In Figure 7, the gradient-based scalar flow properties such as vorticity and energy dissipation are displayed. The spatial dimensions of the flow field were normalized by the bar pitch of 80 mm and the axial length of the cascade's blades which would be placed in the bar wakes. The two key parameters, which were motivated for a comparison with numerical predictions, are the stream-wise vorticity $Vort_Z$ and the dissipation rate of the kinematic energy ε. The stream-wise vorticity in the x/y-plane is calculated from the transformed vector field according to Eq. 2.

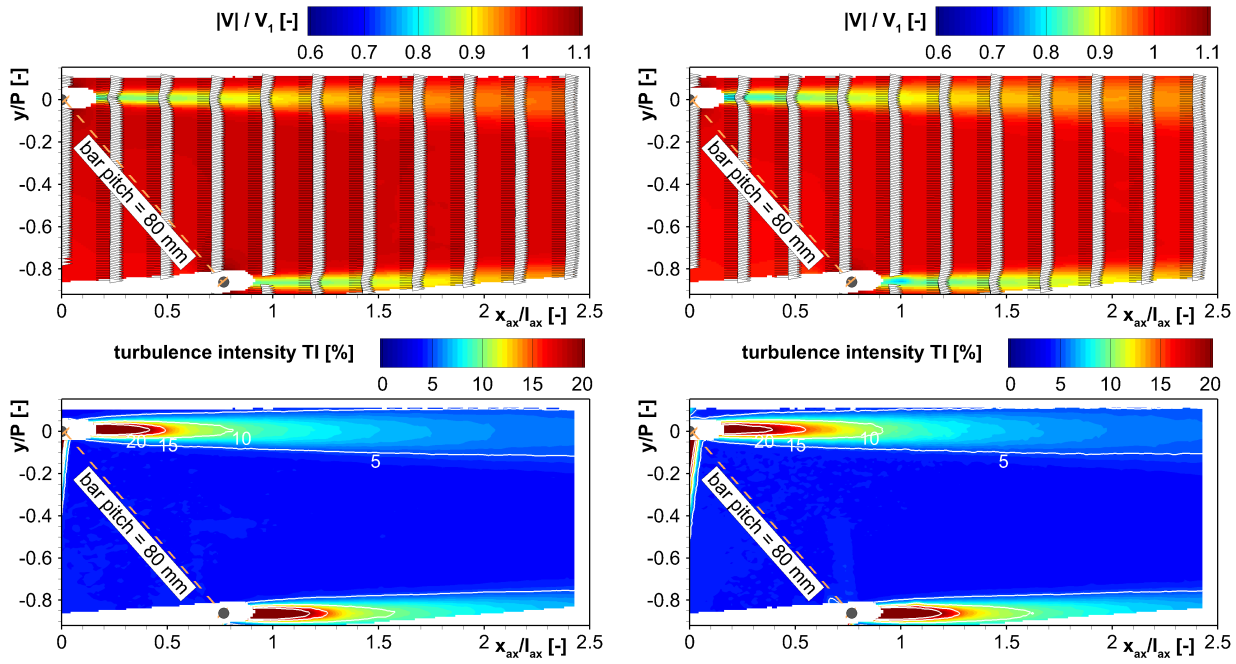

Figure 6: The ensemble-averaged velocity magnitude normalized by the pneumatic wind tunnel velocity $|V|/V_1$ (*top*) and the turbulence intensity TI (*bottom*) are shown color-coded for Re = 60.000 (*left*) and Re = 120.000 (*right*) over one bar pitch. The horizontal vector resolution is reduced by a factor of 10.

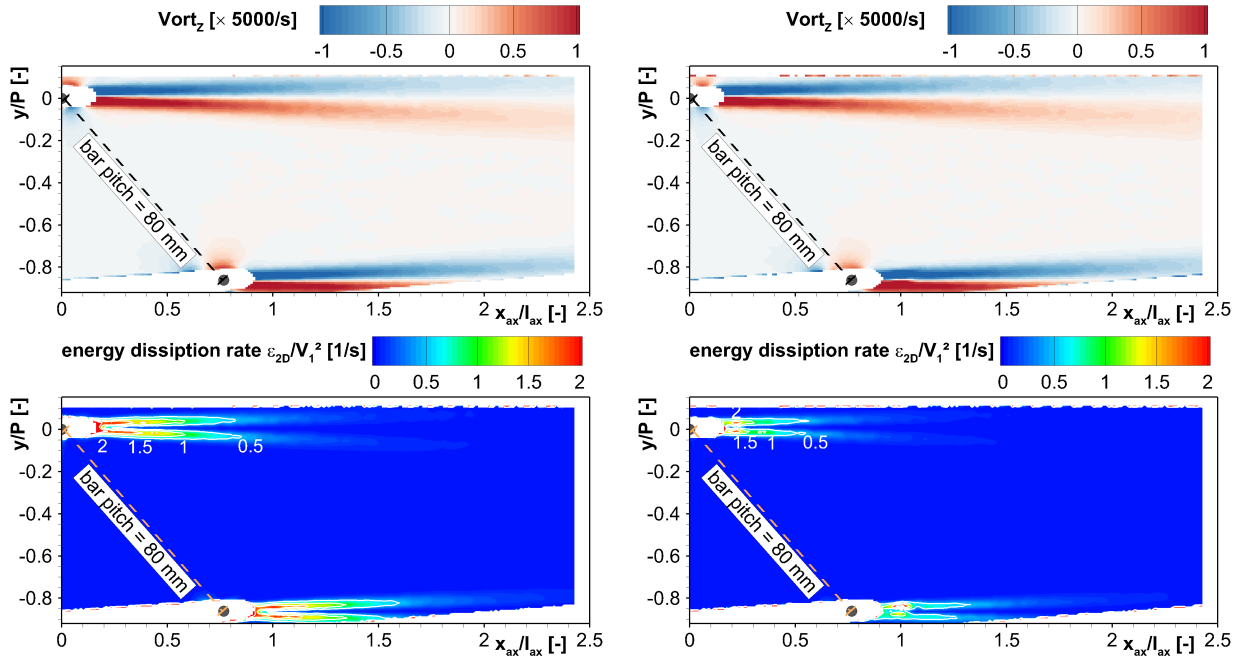

Figure 7: The ensemble-averaged stream-wise vorticity $Vort_Z$ (*top*) and the normalized energy dissipation rate ε_{2D}/V_1^2 (*bottom*) are shown color-coded for Re = 60.000 (*left*) and Re = 120.000 (*right*) over one bar pitch.

$$Vort_Z = (\frac{\partial v}{\partial x} - \frac{\partial u}{\partial y})\vec{z} \tag{2}$$

The energy dissipation rate is usually referring to the full 3D velocity tensor. As the flow field is planar (or 2D) at this position, the dissipation rate of the kinetic energy can be calculated by applying Eq. 3 according to Hinze (1975). The kinematic viscosity was calculated by using the thermodynamic state variables for each operating point.

$$\varepsilon = \nu\left[3\left\{\left(\frac{\partial u}{\partial x}\right)^2 + \left(\frac{\partial v}{\partial y}\right)^2\right\} + 3\left\{\left(\frac{\partial u}{\partial y}\right)^2 + \left(\frac{\partial v}{\partial x}\right)^2\right\} + 6\left\{\left(\frac{\partial u}{\partial u}\frac{\partial v}{\partial u}\right)\right\}\right] \tag{3}$$

As outlined from the figures, the flow field in the wake of the bars establishes like expected with some minor differences regarding to Reynolds number effects. The recirculation in the vicinity of the bar, which extends roughly half an axial length or about 25 mm downstream of the bar, provides strong fluctuations and high turbulence intensity of more than 25 %. The free-stream turbulence intensity apart from the bar wakes is about 3.8 %, matching both, the results from hot-wire anemometry as mentioned earlier in the text as well as from the authors in Kirik and Niehuis (2015). The scalar flow quantities are comparable for both bars within the field of view, what indicates good periodicity in the flow field. The recirculation region for the higher Reynolds number is slightly slender and shorter what is expected from other studies on separating/reattaching flows, compare e.g. Bai and Alam (2018) or Bitter et al. (2011). In Figure 8, the scalar distribution of the turbulence intensity, the stream-wise vorticity and the corresponding local measurement uncertainty is shown exemplary from a cut 25 mm downstream from the

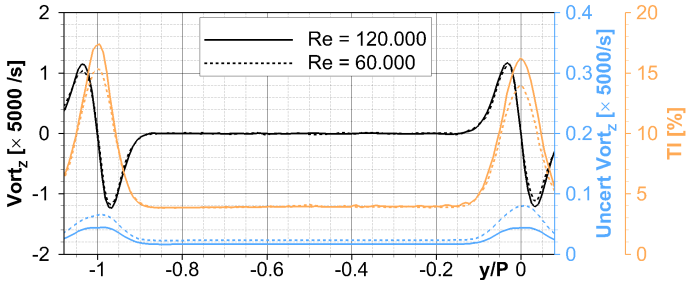

Figure 8: Comparison of the stream-wise vorticity, the uncertainty and the turbulence intensity over one bar pitch 50 mm downstream of the bars for both operating points.

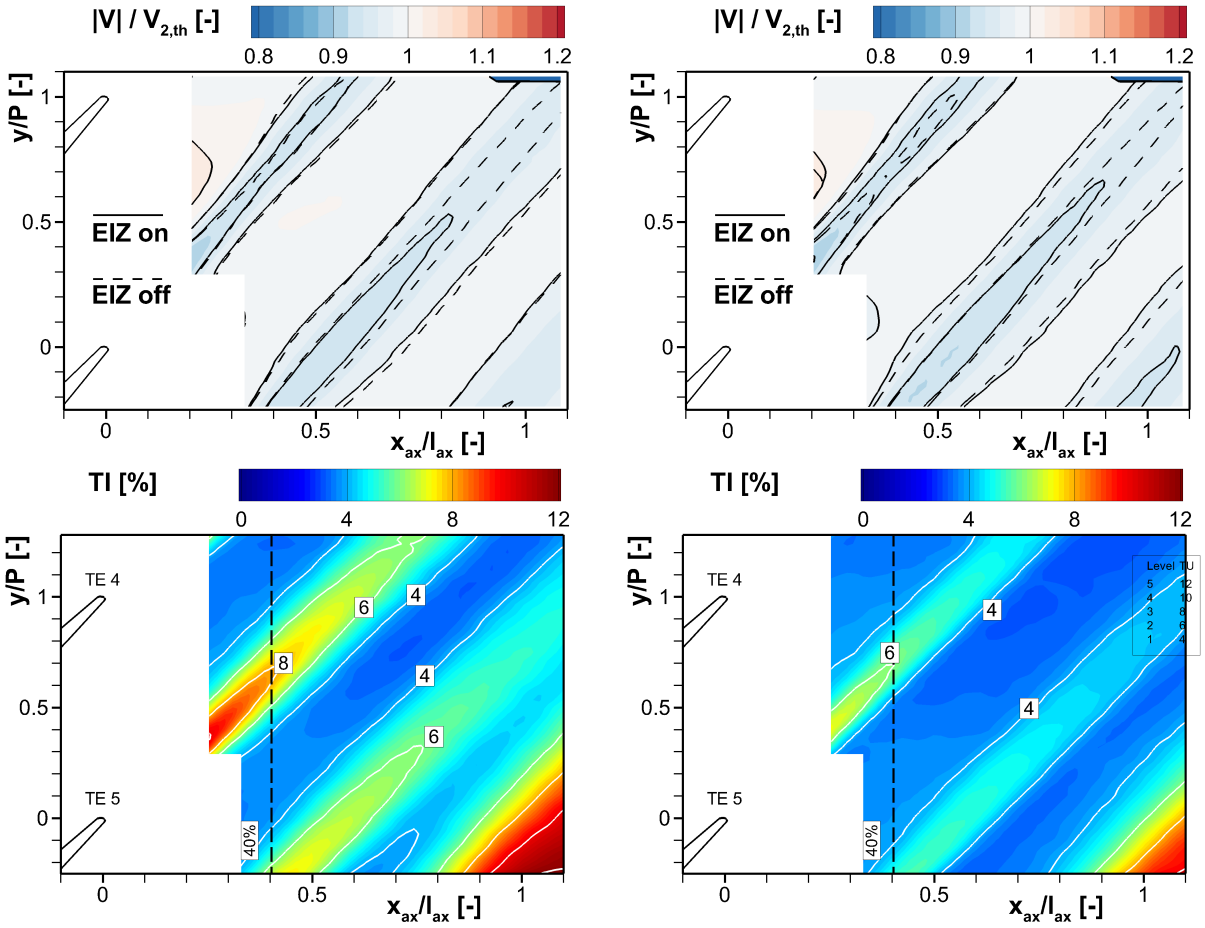

Figure 9: Ensemble-averaged velocity magnitude field $|V|/V_{2,th}$ (*top*) and turbulence intensity TI (*bottom*) in the wake of LPT blade 5 and 6 for Re = 60.000 (*left*) and Re = 120.000 (*right*). The normalization value was the theoretical exit velocity $V_{2,th}$.

bars parallel to the plane indicated by the dashed line ("bar pitch = 80 mm") in the previous figures. For the higher Reynolds number, the peak turbulence intensity as well as the peak vorticity is slightly stronger. The measurement uncertainty was derived from the the noise level and the shape of the peak in the correlation plane. The procedure is implemented in the PIV processing suite whereas the approaches are described in more detail in Wieneke (2017). As the tracer particle concentration increases with rising ambient pressure (i.e. Reynolds number) in the facility, the reduction of the statistical error is also expected as shown. The order of magnitude as well as the topology of the quantities shown downstream of the bars, which act as inflow wake generators for the LPT cascade, help to quantify the effects on the wake flow downstream of the blades in the following chapter.

4 Results of the Wake Investigations

4.1 Period-averaged flow fields

The period-averaged flow field, which is the average of the total number of samples ($= 10\,\text{timesteps} \cdot 1.000\,\text{samples}$), is shown in Figure 9 for an activated wake generator (EIZ on). The normalized absolute velocity field (*top*) and the turbulence intensity (*bottom*) downstream of the trailing edges of blade 5 and 6 are shown color-coded for Re = 60.000 (*left*) and Re = 120.000 (*right*). The dashed lines in the top figures indicate the flow topology of the deactivated wake generator (EIZ off) for comparison. Similar to the previous chapter, the spatial coordinates were normalized with the axial blade chord length l_{ax} and the blade pitch P in x- and y-direction, respectively. Unfortunately, strong reflections at the blades trailing edge impeded the data evaluation up to $x_{ax}/l_{ax} \approx 0.25$ due to poor SNR.
An aerodynamic characteristic of this LPT blade is the development of a separation bubble in the decelerating flow regime on the rear part of the suction surface. The bubble size reduces with increasing Re. Hence,

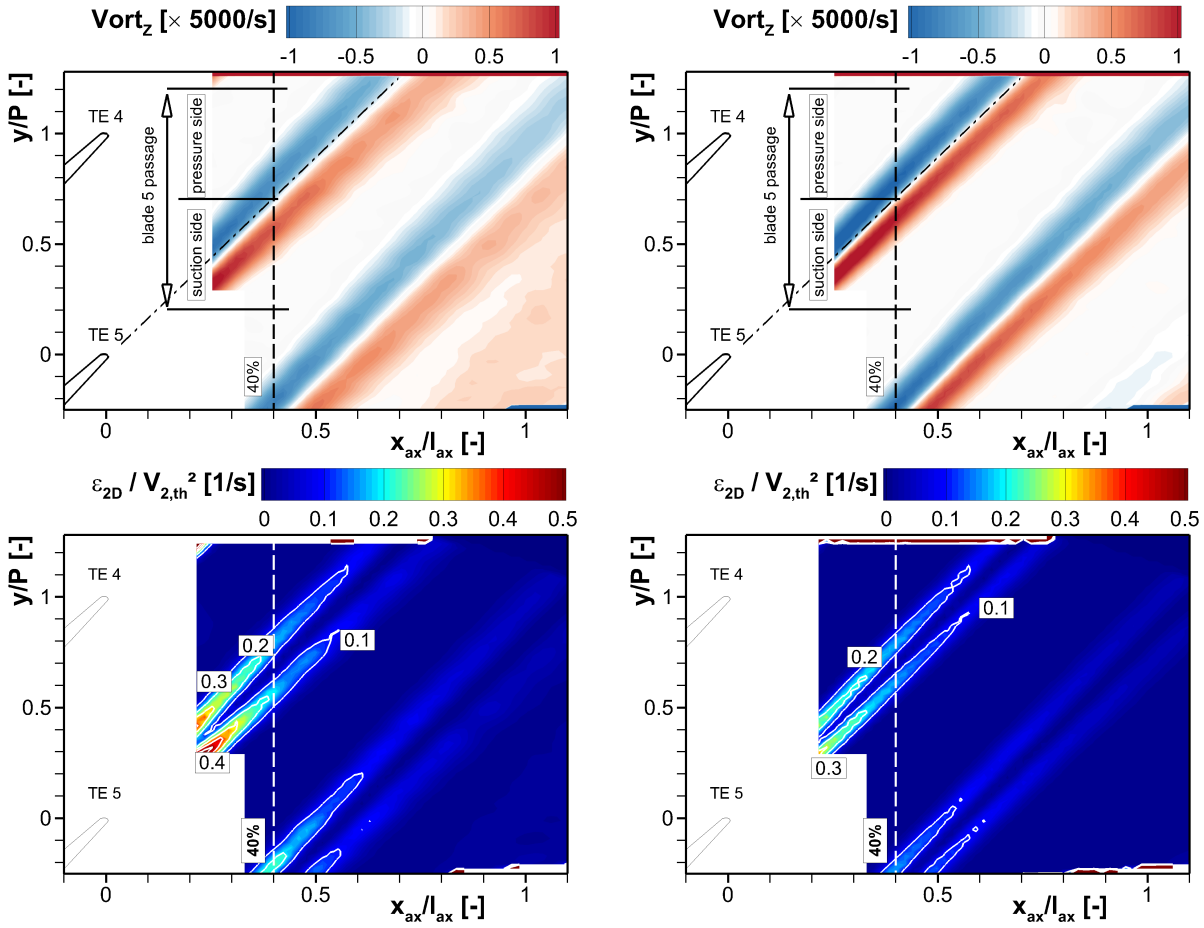

Figure 10: Ensemble-averaged vorticity field (*top*) and kinematic energy dissipation rate $\varepsilon_{2D}/V_{2,th}^2$ (*bottom*) in the wake of LPT blade 5 and 6 for Re = 60.000 (*left*) and Re = 120.000 (*right*) for moving *EIZ*. The normalization value was the theoretical exit velocity $V_{2,th}$.

the blade losses increase as a consequence of the wake widening and the rising turbulent interaction in the shear layer. This effect can be identified in the topology of the turbulence intensity field. The wake is wider and exhibit stronger absolute values for the small Reynolds number, compare. e.g. Bai and Alam (2018) or Ciorciari et al. (2014). The turbulence intensity apart from the wake is in the order of the inflow turbulence level around 4 %.

The differences due to the Reynolds number effect can also be shown in the gradient-based scalar quantities. In Figure 10, the vorticity (*top*) and the kinematic energy dissipation rate (*bottom*) are shown for the 2 Reynolds numbers, which indicate a wider wake velocity deficit for the smaller Re number. The vorticity field enables a precise estimation of a virtual separation line between the effects, which were produced either on the blade's suction or pressure side. This position y_{rel}, e.g. at 40 % downstream of the blade, was estimated by the zero-crossing of the vorticity distribution. The periodic inflow effects, i.e. the phase-averaged results, are further discussed in the following chapter by using this definition.

4.2 Effects of Periodic Inflow

The period-averaged results from the previous section are used in the following to separate the effects of the incoming periodic wakes. Therefore, the phase-averaged data for each of the 10 bar period time steps τ/T were reduced by the corresponding period-averaged value. In Figure 11, the development of the turbulence intensity (*top*) and the kinematic dissipation rate (*bottom*) are shown for both Reynolds numbers (low *left* and high *right*). The data was extracted at 40 % axial distance as outlined in the previous section. The development of the periodic effect is shown for 1 blade pitch (blade 5, $-0.5 \leq y/P_{rel} \leq 0.5$), whereas $y/P_{rel} \leq 0$ represent the suction side and $y/P_{rel} \geq 0$ the pressure side, respectively. Flow patterns, on average, propagate

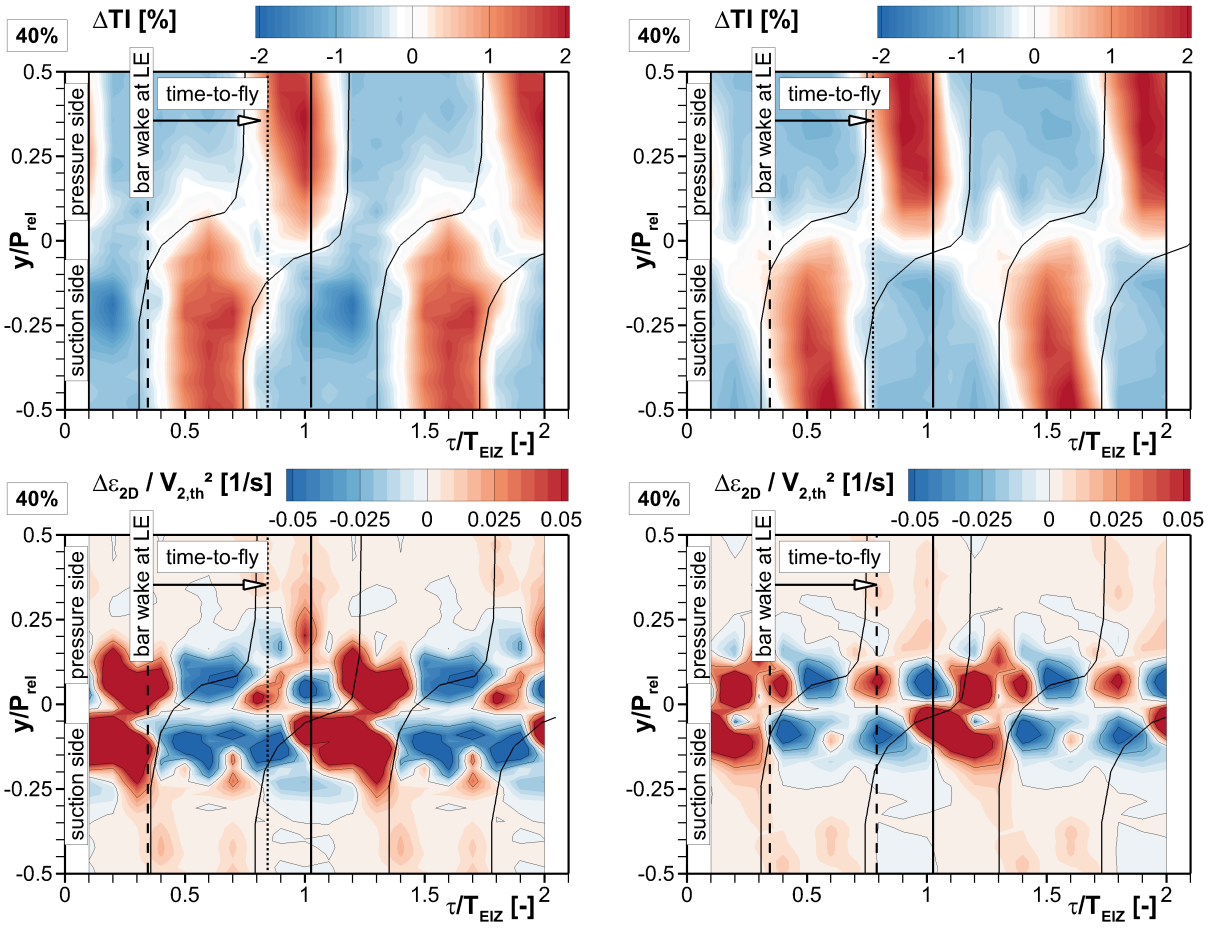

Figure 11: Effect of periodic inflow on the turbulence intensity (*top*) and the kinematic energy dissipation rate (*bottom*) downstream of LPT blade 5 at 40 % axial distance for Re = 60.000 (*left*) and Re = 120.000 (*right*). The plots show the temporal development of differences between the phase-averaged quantities diminished by the period-averaged values for 10 bar period time steps τ/T. The period $\tau/T > 1$ is duplicated.

from the bar through the blade passage down to the plane at 40 % axial distance with an average *time-to-fly* of roughly 1 ms or $\tau/T \approx 0.50$. This value helps to identify the "delay" on either the suction or pressure side. The bar propagates from the suction to the pressure side as demonstrated in Figure 3. The position *bar wake at leading edge* indicates the delay in the plots, which must be considered regarding the *time-to-fly*.
As outlined from the figures, the peak turbulence intensity increases by roughly 2 % in comparison to the period average as a consequence of the turbulent bar wake which propagates through the passage. The energy dissipation rate reveals, that the wake extends over approximately $-0.2 \leq y/P_{rel} \leq 0.2$, whereas the peak values occur in the center of the shear layer at $y/P_{rel} = \pm 0.1$. As a consequence of the bar wakes propagating along the suction side, the dissipation rate increases in the free-stream parts of the passage at $|y/P_{rel}| \geq 0.25$. In turn, the dissipation rate decreases inside the wake region at $|y/P_{rel}| \leq 0.2$ at the same time. This is the consequence of the turbulence increase on the suction side, which leads to an earlier transition and a reduced separation bubble size. Consequently, the blade losses and so the dissipation rate downstream of the blade decrease as expected. At $\tau/T \approx 0.85$, the delayed information of the bar located directly upstream the leading edge can be seen. Beyond this time step, the perturbation changes from the suction to the pressure side passage. This change leads to an increased dissipation rate in the wake facing the pressure side for both Reynolds numbers. As a consequence of the bar wake deficit, the incidence angle on the blade slightly changes to either a pressure or suction side incidence depending on the relative bar position. This causes a stronger or weaker aerodynamic loading of the airfoil what, in turn, has a periodic effect on the dissipation rate in the wake.
For a comparison with numerical predictions, especially for unsteady or time-resolved simulations, the con-

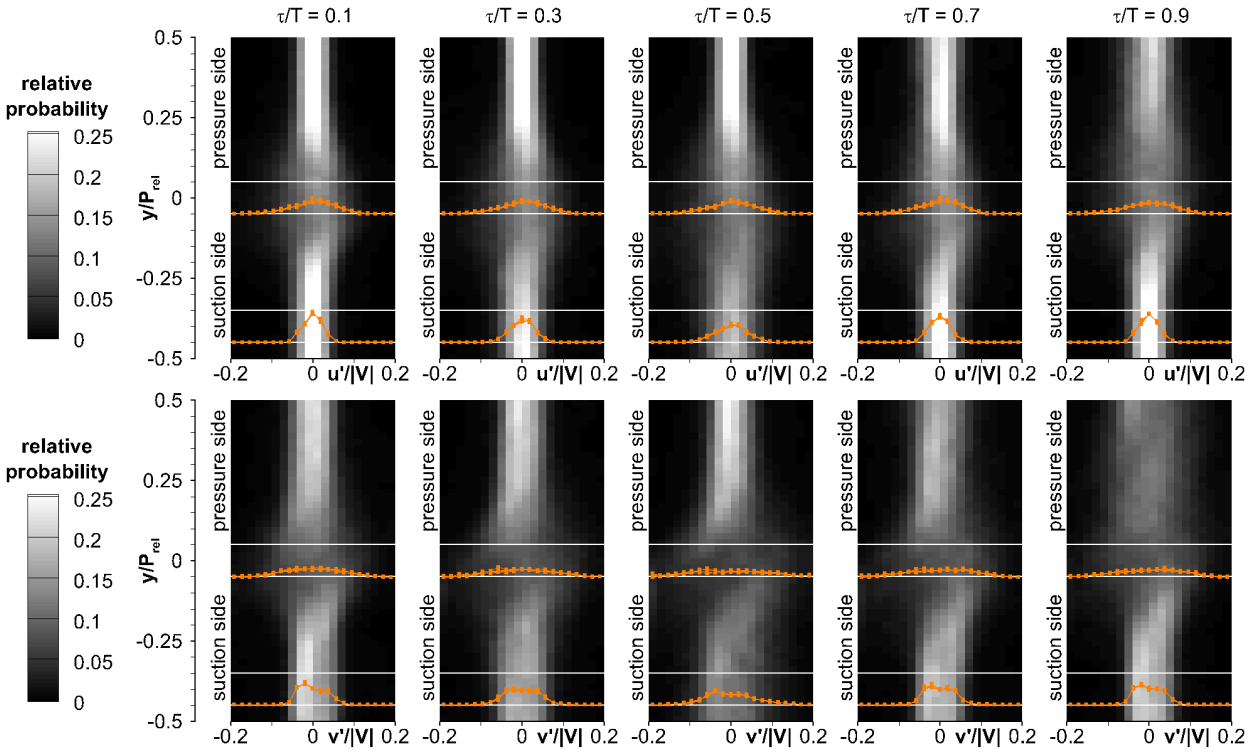

Figure 12: Probability density function of stream-wise velocity fluctuations u'/V (*top*) and v'/V (*bottom*) for 5 time steps at Re = 60.000. Origin of turbulent quantities from Figure 11.

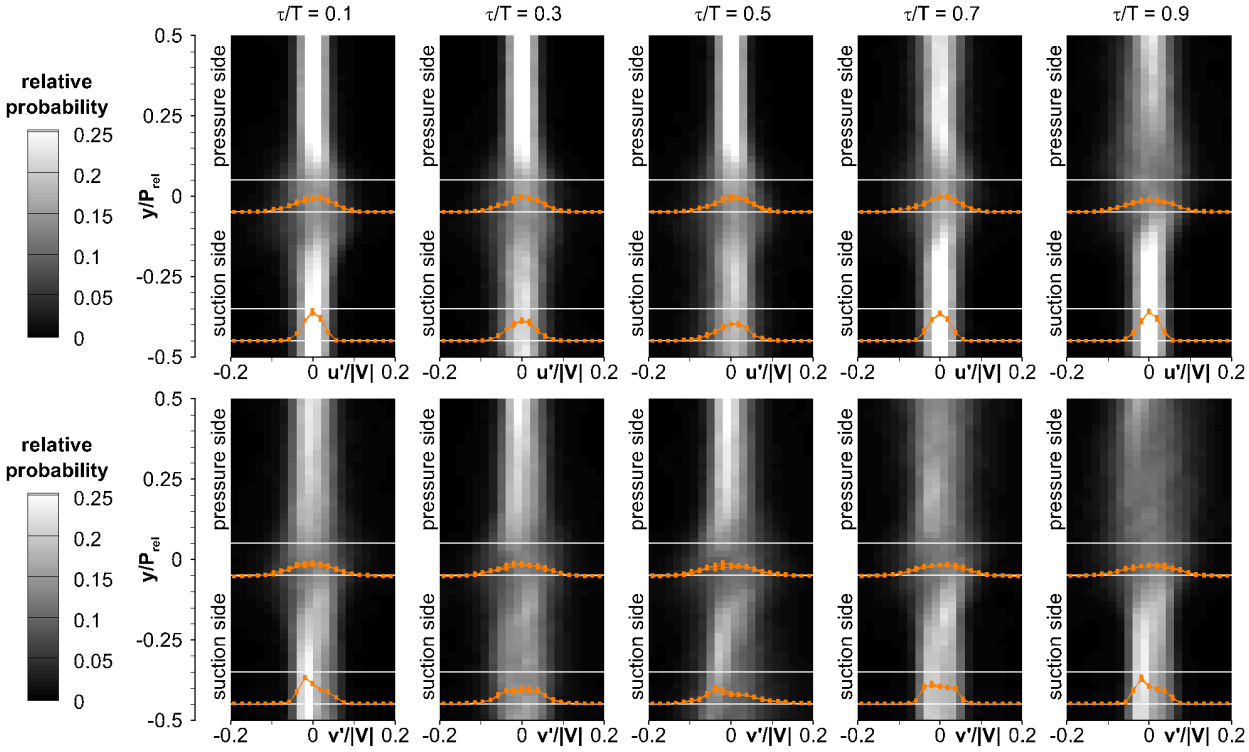

Figure 13: Probability density function of stream-wise velocity fluctuations u'/V (*top*) and v'/V (*bottom*) for 5 time steps at Re = 120.000. Origin of turbulent quantities from Figure 11.

formity of statistical quantities such as u'/V and v'/V between simulations and experiments is from fundamental interest. The representation of statistical values in numerical methods can be an indicator of too high or low damping of turbulent fluctuations and, hence, on the under- or over-estimation of fluctuation-induced flow regimes such as wakes, shear layers and re-attachment regions. In order to present an impression of the distribution of the stream-wise turbulent fluctuations u'/V and v'/V, the local probability density functions (*PDF*) over the pitch of blade 5 at 40 % axial distance are shown as gray-shaded aerial distribution in Figure 12 and 13 for Re = 60.000 and Re = 120.000, respectively. The PDFs are shown for five time steps of the period starting with $\tau/T = 0.1$, whereas the delta is $\Delta\tau/T = 0.2$. Two line-plots (orange) are included in each plot, representing a cut-out from the corresponding map, i.e. a PDF in the center of the pitch at $y/P_{rel} = 0$ and close to the outer suction side passage at $y/P_{rel} = -0.45$. The corresponding white lines around each line-plot represent the minimum and maximum values of the gray-scale color map of the entire plot for a better ranking in the context of the whole figure. Each PDF was calculated from the fluctuation values $V' = (V - \overline{V})_{phase}$ of 1.000 samples for each time step, whereas $V' = [u'; v']$. It can be distinguished between the following differences in the topology of the individual PDFs: a) the PDF of the axial component u' is widely symmetric, whereas the PDF of the lateral component v' shows a certain negative skewness. Since the lateral velocity fluctuations v' are superimposed by the lateral velocity component of the wake generator, a preferential negative orientation is conceivable. b) The PDFs of the axial component $u'/|V|$ inside the blade wake at $|y/P_{rel}| \leq 0.2$ are broader compared to the free-stream regime in the rest of the passage. This is expected from dominant vortex shedding in the vicinity of trailing edges in comparison to free-stream turbulence in turbomachinery, see Walker (1993). At time steps $\tau/T = 0.5$ or $\tau/T = 0.9$, where the peak turbulence increase is present either on the suction or on the pressure side, the PDFs of both fluctuation components are significantly influenced as a consequence of the periodic perturbation. The eddies inside the periodic wakes are more dominant and less dissipated compared to the free-stream. Despite the damping during the flow acceleration across the blade, larger and stronger structures are still measurable in the wake. The influence is stronger noticeable for the lateral component v' as for u'.

5 Conclusions

The intention of the work was the experimental characterization of the turbulent in- and outflow on a linear low-pressure turbine cascade under periodic inlet conditions by applying the PIV measurement technique. Stereoscopic PIV measurements were performed to investigate the flow in the vicinity of a wake generator which was equipped with 2 mm cylindrical bars. The measurements were targeted to deliver the LPT cascade inflow turbulence intensity and the stream-wise vorticity from wakes which simulate an upstream blade row. At the outlet of the linear cascade, the phase-locked PIV technique was used to explore the quasi-temporal effect of the inlet perturbations on the flow statistics in the wake. Especially, the development of the turbulence intensity and the kinematic dissipation rate were from interest.

An application of the PIV measurement technique is challenging under such conditions as presented here. The low ambient pressure as well as the high-speed flow at the exit of the cascade require a very careful measurement procedure from beginning with of the setup until the post-processing of the results. Nevertheless, it was demonstrated, that the PIV technique can deliver reliable and robust results of turbulent quantities from both, the stereoscopic and phase-locked measurements under such conditions.

The periodicity of the flow field around the bars from the wake generator as well as the two-dimensional character of the flow was validated with the stereoscopic measurements. The wake turbulence intensity in the free-stream as well as its peak value of up to 25 % match with the literature as also with reference data from previous measurements. The period-averaged results of the phase-locked measurements showed that the turbulence intensity at the outlet of the cascade increases periodically by about 2 % as a consequence of the incoming wakes. The periodic change of turbulence intensity forces an intermittent change in the suction side transition. This, in turn shows periodic effects on the kinematic energy dissipation in both, the blade's wake center and the outer regions of the passage. The periodic perturbation, of course, has also an temporal effect on the distribution of the statistical quantities as demonstrated by means of the local probability density function downstream the blade. The character of the PDF, i.e. width and kurtosis, is changed in the presence of a periodic wake.

The performed experiments deliver a deeper insight into the magnitude of periodic perturbations which propagate through an LPT passage. The availability of both, statistical and quasi-temporal data, enables a comprehensive numerical validation whereas the experimental results additionally deliver a comprehensive data base further interpretation of numerical results. The access of the flow field inside the blade's passage at exactly the same operating conditions with the benefits of the experimental methods presented here is challenging. Consequently, simulations might help to close the gap and deliver the full extend from propagating turbulent structures in the full extend.

Acknowledgements

The authors would like to thank MTU Aero Engines for the financial and intellectual support to realize this research effort.

References

Acton P and Fottner L (1996) The generation of instationary flow conditions in the high-speed cascade wind tunnel. in *13th Symposium on Measuring Techniques in Transonic and Supersonic Flow in Cascades and Turbomachines, Zürich, Switzerland, September 5-6*

Acton P and Fottner L (1998) Investigation of the Boundary Layer Development on a Highly Loaded Low Pressure Turbine Cascade Under the Influence of Unsteady Flow Conditions. in TH Fransson, editor, *Unsteady Aerodynamics and Aeroelasticity of Turbomachines*. pages 393–406. Springer Netherlands, Dordrecht

Bai H and Alam MM (2018) Dependence of square cylinder wake on Reynolds number. *Physics of Fluids* 30:015102

Bitter M, Kurz J, Kähler C, and Niehuis R (2016) Investigations of a low-pressure turbine blade by means of simultaneous optical velocity and pressure measurements. in *18th International Symposium on Applications of Laser Techniques to Fluid Mechanics, Lisbon, Portugal, July 4-7*

Bitter M, Scharnowski S, Hain R, and Kähler CJ (2011) High-repetition-rate PIV investigations on a generic rocket model in sub- and supersonic flows. *Experiments in Fluids* 50:1019–1030

Breuer M (2018) Effect of Inflow Turbulence on an Airfoil Flow with Laminar Separation Bubble: An LES Study. *Flow, Turbulence and Combustion* 101:433–456

Brunner S and Fottner L (1999) Untersuchungen zum Einflußder Rotor-Stator Interaktion auf die saugseitige Transition eines hochbelasteten ungekühlten Niederdruck-Turbinengitters. in *DGLR Jahrestagung, DGLRJT99-078, Berlin, 27.-30. September*

Chemnitz S and Niehuis R (2019) A comparison of turbulence levels from PIV and CTA downstream of a low-pressure turbine cascade at high-speed flow conditions. in *ASME Turbo Expo, GT 2019-90473, Phoenix, Arizona, USA, June 17-21*

Ciorciari R, Kirik I, and Niehuis R (2014) Effects of Unsteady Wakes on the Secondary Flows in the Linear T106 Turbine Cascade. *Journal of Turbomachinery* 136:091010–091010–11

Dróżdż A and Uruba V (2014) Comparison of PIV and Hot-Wire statistics of turbulent boundary layer. *Journal of Physics: Conference Series* 530:012044

Gomes-Fernandes R, Ganapathisubramani B, and Vassilicos JC (2012) Particle Image Velocimetry Study of Fractal-generated Turbulence. *Journal of Fluid Mechanics* 711:306–336

Herbst SL, Kähler CJ, and Hain R (2017) SD7003 Airfoil in Large-scale Free stream Turbulence. in *35th AIAA Applied Aerodynamics Conference, Denver, Colorado, USA, June 5-9*

Hinze JO (1975) *Turbulence*. New York, N.Y. : McGraw-Hill. 2nd edition

Kähler CJ, Astarita T, Vlachos PP, Sakakibara J, Hain R, Discetti S, La Foy R, and Cierpka C (2016) Main results of the 4th International PIV Challenge. *Experiments in Fluids* 57:97

Kirik I and Niehuis R (2015) Comparing the Effect of UnsteadyWakes on Parallel and Divergent Endwalls in a LP Turbine Cascade (T106A-EIZ and T106D-EIZ). in *11th International Gas Turbine Congress, Tokyo, Japan, November 15-20*

Mahallati A and Sjolander SA (2012) Aerodynamics of a Low-Pressure Turbine Airfoil at Low Reynolds Numbers Part II: Blade-Wake Interaction. *Journal of Turbomachinery* 135:011011–1–10

Scharnowski S, Bross M, and Kähler CJ (2018) Accurate turbulence level estimations using PIV/PTV. *Experiments in Fluids* 60:1

Scholz N and Hopkes U (1959) Der Hochgeschwindigkeits-Gitterwindkanal der Deutschen Forschungsanstalt für Luftfahrt Braunschweig. *Forschung auf dem Gebiet des Ingenieurwesens A* 25:133–147

Stieger RD and Hodson HP (2005) The Unsteady Development of a Turbulent Wake Through a Downstream Low-Pressure Turbine Blade Passage. *Journal of Turbomachinery* 127:388 – 394

Sturm W and Fottner L (1985) The High-Speed cascade Wind-Tunnel of the German Armed Forces University Munich. in *8th Symposium for Measurement Techniques in Transonic and Supersonic flows in Cascades and Turbomachinery, MTT0885-A102, Genoa, Italy, October 24-25*

Talan M and Hourmouziadis J (2002) Characteristic Regimes of Transitional Separation Bubbles in Unsteady Flow. *Flow, Turbulence and Combustion* 69:207–227

Walker G (1993) The Role of Laminar-Turbulent Transition in Gas Turbine Engines: A Discussion. *Journal of Turbomachinery* 115:207 – 216

Wieneke BF (2017) *PIV Uncertainty Quantification and Beyond*. Dissertation. Delft Technical University